Suplemento de la Revista Mexicana de Física **3** 0308042 (2022) 1–5

On the nature of $X(6900)$ and other structures in the LHCb di-j/ψ spectrum

Ze-Rui Liang and De-Liang Yao*

School of Physics and Electronics, Hunan University, 410082 Changsha, China.
**e-mail: yaodeliang@hnu.edu.cn*

Received 14 January 2022; accepted 1 March 2022

The LHCb di-J/ψ spectrum is studied within the framework of effective field theory with four coupled channels $\{J/\psi J/\psi,\ J/\psi\psi(2S),\ J/\psi\psi(3770),\ \psi(2S)\psi(2S)\}$, in order to unveil possible underlying fully-charmed tetraquark states. The partial-wave analysis is performed properly, and the unitarity of the scattering amplitudes is restored via Bethe-Salpeter equation under on-shell approximation. Four states are found in the energy region $[6.2\ \mathrm{GeV}, 7.6\ \mathrm{GeV}]$. For the partial wave with quantum numbers 0^{++}, a bound state $X(6200)$ and a narrow resonance $X(7200)$ can be dynamically generated, while for the 2^{++} partial wave, two different resonant states, one named $X(6900)$ with a narrow width and the other $X(6680)$ with a broad width, can be found. Our results of the mass and width of $X(6900)$ agree well with the experimental ones given by the LHCb collaboration. Furthermore, our findings shed first light on the determination of the J^{PC} quantum numbers of these states.

Keywords: Partial-wave analysis; exotic states.

DOI: https://doi.org/10.31349/SuplRevMexFis.3.0308042

1. Introduction

In 2020, the LHCb collaboration declared the discovery of a new XYZ member with a narrow width, denoted by $X(6900)$, in the J/ψ-pair invariant mass spectrum around $6.9\ \mathrm{GeV}$ [1]. The measured mass and width of $X(6900)$ are given by two scenarios. The results for scenario I with interference are $\mathrm{M}[X(6900)] = 6886 \pm 11 \pm 11\ \mathrm{MeV}$, $\Gamma[\mathrm{X}(6900)] = 168 \pm 33 \pm 69\ \mathrm{MeV}$, while for scenario II without interference, $\mathrm{M}[X(6900)] = 6905 \pm 11 \pm 7\ \mathrm{MeV}$, $\Gamma[\mathrm{X}(6900)] = 80 \pm 19 \pm 33\ \mathrm{MeV}$. Note that hints of a broad structure above the J/ψ-pair threshold and a possible structure around $7.2\ \mathrm{GeV}$ were also observed by the LHCb collaboration.

Since it is the first confirmation of a fully-charmed multiquark candidate in experiments, it immediately attracted intensive attentions from both theoreticians and experimentalists. On the theoretical side, plenty of works are dedicated to decipher the inner structure, J^{PC} numbers or other properties of the related fully-charmed states $T_{cc\bar{c}\bar{c}}$, through the methods such as quark model [2–5], QCD sum rule [6–9], non-relativistic QCD factorization [10–12] and phenomenological models [13–18].

In order to reveal possible states in the J/ψ-pair spectrum in the range of $[6.2\ \mathrm{GeV}, 7.6\ \mathrm{GeV}]$ and to pin down their J^{PC} numbers, we constructed the production amplitudes of di-J/ψ in the pp collision, and incorporated the effect of final state interaction in a coupled-channel way. There are several channels, such $\eta_c\eta_c$, h_ch_c, $\chi_{cJ}\chi_{cJ'}$ or $\psi(nS)\psi(n'S)$ pairs ($n, n' = 1, 2, 3\cdots$), which can couple to the J/ψ pair. However, by constructing a generic Lagrangian abiding by the heavy quark spin symmetry (HQSS), we found that the contributions from $\eta_c\eta_c$, h_ch_c and $\chi_{cJ}\chi_{cJ'}$ channels are either suppressed by HQSS or negligible compared to the $\psi(nS)\psi(n'S)$ channels in the meson-exchange picture. Therefore, we only consider the four coupled channels, $\{J/\psi J/\psi,\ J/\psi\psi(2S),\ J/\psi\psi(3770),\ \psi(2S)\psi(2S)\}$, in our analysis.

In this proceeding,[i] we review the work done in Ref. [19], where the partial-wave analysis is employed to reveal possible states in the di-charmonium spectroscopy and to explore their corresponding J^{PC} numbers.

2. Coupled-channel potentials and unitarity

The charmonium scattering processes can be denoted by $V_1(p_1, \varepsilon_1) + V_2(p_2, \varepsilon_2) \to V_3(p_3, \varepsilon_3) + V_4(p_4, \varepsilon_4)$ with momenta p_i and polarization vectors $\varepsilon_i (i = 1, 2, 3, 4)$ specified in the parentheses. The relativistic effective Lagrangian is given in Ref. [19], and the general form of the potentials is

$$V_{ij} = \mathcal{C}_1 \varepsilon_1 \cdot \varepsilon_2 \varepsilon_3^\dagger \cdot \varepsilon_4^\dagger + \mathcal{C}_2 \varepsilon_1 \cdot \varepsilon_3^\dagger \varepsilon_2 \cdot \varepsilon_4^\dagger + \mathcal{C}_3 \varepsilon_1 \cdot \varepsilon_4^\dagger \varepsilon_2 \cdot \varepsilon_3^\dagger \,,$$

where ij are channel indices. The coefficients $\mathcal{C}_{1,2,3}$ are combinations of the low-energy constants (LECs) $h_i (i = 1, 2, \cdots, 9)$ and $h'_j (j = 4, 5, 6, 8)$ appearing in the effective Lagrangian, see Table. I of Ref. [19] for more details.

The definition of helicity amplitude is

$$\begin{aligned} V_{\lambda_1\lambda_2\lambda_3\lambda_4} &= \varepsilon_3^{\rho\dagger}(p_3, \lambda_3)\varepsilon_4^{\sigma\dagger}(p_4, \lambda_4) \\ &\quad \times V_{\mu\nu\rho\sigma}\varepsilon_1^{\mu}(p_1, \lambda_1)\varepsilon_2^{\nu}(p_2, \lambda_2) \,. \end{aligned}$$

Here, the channel labels ij are omitted for the sake of brevity. The helicity eigenvalues $\lambda_i (i = 1, 2, 3, 4)$ can take the values of $\pm 1, 0$. The total number of helicity amplitudes is 81. However, by enforcing P and T parity symmetries, there are only 25 independent helicity amplitudes. The dynamical information is encoded in the amplitude $V_{\mu\nu\rho\sigma}$ that is obtainable from the effective Lagrangian.

We perform partial-wave projection of the helicity amplitudes via the following explicit form

$$V^J_{\lambda_1\lambda_2\lambda_3\lambda_4}(s) = \frac{1}{2}\int_{+1}^{-1} dx V_{\lambda_1\lambda_2\lambda_3\lambda_4}(s,t(s,x)) d^J_{\lambda\lambda'}(x) \,,$$

where s,t are Mandelstam variables and $x=\cos\theta$ with scattering angle θ. $d^J_{\lambda\lambda'}(x)$ is the standard Wigner function with $\lambda=\lambda_1-\lambda_2$ and $\lambda'=\lambda_3-\lambda_4$.

In present work, we only consider S-wave for which the orbital angular momentum is $L=0$. Then the total angular momentum J is equal to the spin S, namely $J=S$. For identical particles, the generalized Bose symmetry and the conversation law of angular momentum impose the constraint on J, which connotes that the total momentum J can only take the values of 0 and 2.

However, the partial-wave amplitudes in the helicity basis do not have definite P parity. It is necessary to transfer the helicity basis to JLS basis, and the concrete form reads

$$\mathcal{V}^J(s) = \sum_{\lambda_1\lambda_2\lambda_3\lambda_4} U^J_{\lambda_3\lambda_4}\mathcal{V}^J_{\lambda_1\lambda_2\lambda_3\lambda_4}(s)[U^J_{\lambda_1\lambda_2}]^\dagger \,. \quad (1)$$

The transformation matrix can be obtained by $U^J_{\lambda_1\lambda_2} = (1/\sqrt{2S+1})\langle S_1\lambda_1 S_2 -\lambda_2|S\lambda\rangle$, which is related to the Clebsch-Gordon coefficients concerning the spins of the initial vector mesons, S_1 and S_2. The $U^J_{\lambda_3\lambda_4}$ for the final states can be obtained in the same manner.

For $J=0$, the total spin $S=0$ implies that $|\lambda_1-\lambda_2|=0$, thus the transformation matrix for the partial-wave amplitude 0^{++} only has three non-zero entries:

$$U^{J=0}_{\lambda_1\lambda_2} = \begin{array}{c|ccc} [\lambda_1\lambda_2] & [+1+1] & [\ 0\ 0] & [-1-1] \\ (1\times 1) & \frac{1}{\sqrt{3}} & -\frac{1}{\sqrt{3}} & \frac{1}{\sqrt{3}} \end{array} \,. \quad (2)$$

For $J=2$, the spin angular momentum is $S=2$ so that $|\lambda_1-\lambda_2|$ can be $0,1,2$. Then the index $[\lambda_1\lambda_2]$ has 9 different choices, and the transformation matrix is

$$U^{J=2}_{\lambda_1\lambda_2} = \begin{array}{c|ccc} [\lambda_1\lambda_2] & [+1+1] & [+1\ 0] & [+1-1] \\ (1\times 1) & \sqrt{\frac{1}{30}} & \sqrt{\frac{1}{10}} & \sqrt{\frac{1}{5}} \\ \hline [\lambda_1\lambda_2] & [\ 0+1] & [\ 0\ 0] & [\ 0-1] \\ (1\times 1) & \sqrt{\frac{1}{10}} & \sqrt{\frac{2}{15}} & \sqrt{\frac{1}{10}} \\ \hline [\lambda_1\lambda_2] & [-1+1] & [-1\ 0] & [-1-1] \\ (1\times 1) & \sqrt{\frac{1}{5}} & \sqrt{\frac{1}{10}} & \sqrt{\frac{1}{30}} \end{array} \,. \quad (3)$$

With these two transformation matrices $U^{J=0,2}_{\lambda_1\lambda_2}$, the S-wave amplitudes can be straightforwardly derived.

To restore the unitarity of the amplitude, the Bethe-Salpeter (BS) equation under on-shell approximation is adopted [21, 22]; see *e.g.* Ref. [23, 24] for recent reviews on various unitarization techniques. The explicit form of BS equation is

$$\mathcal{T}^J(s) = \mathcal{V}^J(s)\cdot[1-\mathcal{G}(s)\cdot\mathcal{V}^J(s)]^{-1} \,. \quad (4)$$

For the coupled-channel case, the kernal $\mathcal{V}^J(s)$ is in the matrix form

$$\mathcal{V}^J(s) = \begin{pmatrix} V^J_{11}(s) & \cdots & V^J_{1n}(s) \\ \vdots & \ddots & \vdots \\ V^J_{n1}(s) & \cdots & V^J_{nn}(s) \end{pmatrix} \,, \quad (5)$$

the dimension of the matrix is identical to the number of coupled channels under consideration. Furthermore, $\mathcal{G}(s)$ is a diagonal matrix in the form of

$$\mathcal{G}(s) = \mathrm{diag}\{g_{ii}(s)\} \,, \quad (6)$$

where $g_{ii}(s)$ denotes the two-point loop function in the $i_{\rm th}$ channel [20]. By analytic continuation of the function $g_{ii}(s)$, the analytical unitarized amplitude on various Riemann Sheets (RS) can be defined. Readers are referred to Ref. [19] for the explicit form of $g_{ii}(s)$ and for the definition of RSs. The pole singularities of the unitarized amplitude are usually interpreted as bound states, virtual states or resonances.

3. Production amplitude

The J/ψ pair is produced through proton-proton collision as shown in Fig. 1. The production amplitude contains two types of contributions: one is direct production and the other is indirect one. The form of the production amplitude is

$$\mathcal{M}_1(s) = \mathcal{A}_1(s)[1+\sum_i \gamma_i\mathcal{G}_{ii}(s)\mathcal{T}_{i1}(s)] \,, \quad (7)$$

with direct amplitude $\mathcal{A}_1$ and $\gamma_i=\mathcal{A}_i/\mathcal{A}_1$. The direct amplitude $\mathcal{A}_1$ is the process that directly produces the $J/\psi J/\psi$ pairs. The indirect amplitude takes the rescattering effect of the final state interaction into consideration, where the coupled-channel effects amongst $\{J/\psi J/\psi,\ J/\psi\psi(2S),\ J/\psi\psi(3770),\ \psi(2S)\psi(2S)\}$ are explicitly incorporated.

The expression for the invariant mass formula is given by

$$\frac{d\mathcal{N}}{d\sqrt{s}} = \rho(s)|\mathcal{A}_1(s)|^2\left|\gamma+\sum_i \mathcal{G}_{ii}(s)\mathcal{T}_{i1}(s)\right|^2 \,, \quad (8)$$

which is proportional to the square of the production amplitude, multiplied by a phase space factor $\rho(s) = \lambda^{\frac{1}{2}}(s,m^2_{J/\psi},m^2_{J/\psi})/(16\pi s)$, with the Källén function $\lambda(a^2,b^2,c^2)=[a^2-(b+c)^2][a^2-(b-c)^2]$.

The unit in the second line of Eq. (7) is set as γ, and it is regarded as coherent background contribution. Meanwhile, other γ_i's are taken to be 1 for the purpose of reducing the number of free parameters. Actually, the effect of γ_i's may be absorbed, in part, into the coherent constant γ or the constants involved in the amplitude $\mathcal{T}_{i1}(s)$. In our case, the direct amplitude $\mathcal{A}_1$ is parameterized as the form of [16]

$$|\mathcal{A}_1(s)|^2 = \alpha^2 e^{-2\beta s} \,, \quad (9)$$

where α and β are normalization factor and slope parameter, respectively.

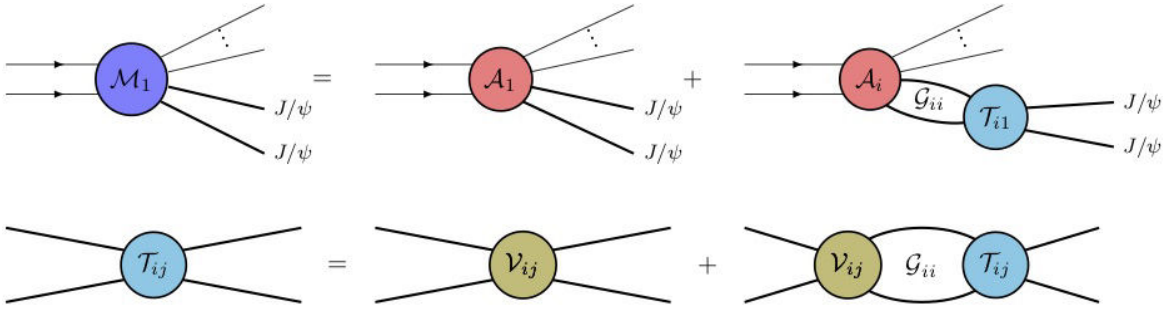

FIGURE 1. Schematic diagram of the production of J/ψ pairs through proton-proton collision. Coupled-channel effects are incorporated via rescatterings of final charmonium states.

TABLE I. Positions and residues of the poles obtained in the four-coupled-channel fits.

RS (J^{PC})	Positions	$\lvert\text{Residue}\rvert^{1/2}$ [GeV]			
	$\sqrt{s_{\text{pole}}}$ [MeV]	$J/\psi J/\psi$	$J/\psi\psi(2S)$	$J/\psi\psi(3770)$	$\psi(2S)\psi(2S)$
I (0^{++})	$6124.8^{+23.9}_{-121.8}$	$24.6^{+7.5}_{-2.3}$	$21.0^{+21.2}_{-6.7}$	$1.1^{+1.1}_{-1.1}$	$2.7^{+18.2}_{-2.6}$
II (2^{++})	$6680.3^{+80.9}_{-53.0} - i136.1^{+39.3}_{-46.4}$	$14.9^{+2.1}_{-2.4}$	$26.5^{+1.8}_{-2.8}$	$7.8^{+5.9}_{-1.7}$	$39.0^{+4.9}_{-5.2}$
VIII (2^{++})	$6919.8^{+17.2}_{-23.7} - i58.8^{+10.9}_{-12.2}$	$5.7^{+1.6}_{-1.3}$	$9.9^{+1.1}_{-1.8}$	$2.9^{+1.2}_{-0.5}$	$52.7^{+1.7}_{-1.1}$
VIII (0^{++})	$7234.3^{+24.2}_{-28.5} - i45.1^{+37.8}_{-20.0}$	$5.6^{+2.1}_{-1.8}$	$6.2^{+1.1}_{-1.1}$	$0.9^{+0.3}_{-0.3}$	$37.0^{+2.6}_{-2.3}$

4. Fits and predictions

We are now in the position to confront our model with the experimental data by the LHCb. We perform partial-wave analysis of J/ψ-pair invariant mass spectrum and hunt for possible states in the entire fitting range with definite J^{PC} numbers of 0^{++} and 2^{++}. Three different kinds of fit are carried out: three-coupled-channel fit, four-coupled-channel fits and combined fit.

We first consider the fits of three coupled channels $\{J/\psi J/\psi,\ J/\psi\psi(2S),\ J/\psi\psi(3770)\}$ with the energy region ranging from 6.2 GeV to 7.2 GeV, which covers the narrow structure around 6.9 GeV and is adequate to reconstruct the experimental spectrum distribution in principle. However, the results show that the three-coupled-channel cases do not make a clear distinction between the 0^{++} and 2^{++} partial-wave amplitudes. Namely, the behaviours of predicted theoretical line-shapes of the two fits, with only 0^{++} or only 2^{++} partial waves, turn out to be indistinguishable. For the three-coupled-channel fits, a bound state near the di-J/ψ threshold can be found, which is referred to as $X(6200)$ [16]. A peak around 6.9 GeV is also seen, but the dominate contribution mainly attributes to the threshold effect of the $J/\psi\psi(3770)$ channel.

Therefore, we extend the fitting range up to the energy 7.6 GeV. In this way, more experimental data are included. Furthermore, we add one extra channel, *i.e.* the $\psi(2S)\psi(2S)$ interaction. By considering four coupled channels $\{J/\psi J/\psi,\ J/\psi\psi(2S),\ J/\psi\psi(3770),\ \psi(2S)\psi(2S)\}$, two different fits (here denoted by Fit-I and Fit-II) are performed, as the cases in the three-channel fits described above. The fit results, together with comparison with the LHCb data, are shown in Fig. 2. It can be seen from the plots that the theoretical predictions of 0^{++} and 2^{++} invariant mass spectrum can be easily distinguished now.

For Fit-I with 0^{++} partial wave, there exists good agreement between our theoretical results and the LHCb data in the energy range $[6.2\ \text{GeV}, 7.6\ \text{GeV}]$. A resonant state is dynamically generated, named as $X(7200)$. It is located in the RS-VIII and the relevant pole position reads

$$\sqrt{s_{\text{pole}}} = (7234.3^{+24.2}_{-28.5} - i45.1^{+37.8}_{-20.0})\ \text{MeV}. \tag{10}$$

From Table I, it can be seen that this state has larger coupling to the $\psi(2S)\psi(2S)$ channel, compared to the other three channels. Also, the enhancement around 7.3 GeV in Fig. 2 exhibits the occurrence of $X(7200)$ state. In addition, a bound state, *i.e.* $X(6200)$, is also obtained

$$\sqrt{s_{\text{pole}}} = 6124.8^{+23.9}_{-121.8}\ \text{MeV}. \tag{11}$$

For Fit-II with 2^{++} partial wave, the fitting quality is excellent below 7.2 GeV, but deviation from the experimental data starts to show up in the vicinity of the energy 7.3 GeV. Two poles of quantum numbers $J^{PC} = 2^{++}$ are found. One is a narrow resonant state, which appears around 6.9 GeV,

$$\sqrt{s_{\text{pole}}} = (6919.8^{+17.2}_{-23.7} - i58.8^{+10.9}_{-12.2})\ \text{MeV}. \tag{12}$$

This state can be identified as the $X(6900)$ state reported by the LHCb collaboration [1]. The coupling constant with the fourth channel of this state is large, indicating that the $\psi(2S)\psi(2S)$ channel takes the major responsibility for the existence of the $X(6900)$ state. On the other hand, a broad resonant structure, dubbed $X(6680)$, is discovered, although its effect is interpreted as the threshold enhancement by the LHCb collaboration [1].

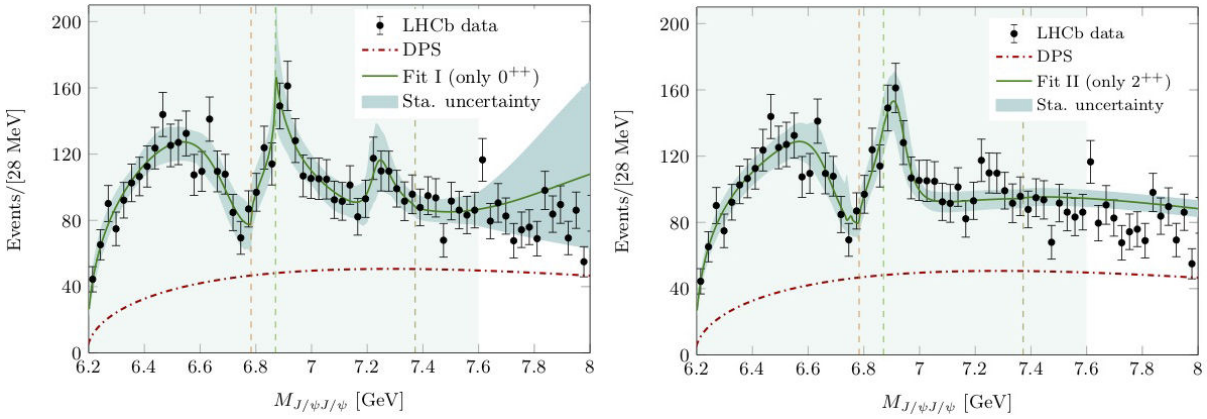

FIGURE 2. Results of four-coupled-channel fits. Left panel: Fit-I with only 0^{++} partial wave; right panel: Fit-II with only 2^{++} partial wave. The dashed lines indicate thresholds, and the light green background stands for the fitting range $[6.2\ \text{GeV}, 7.6\ \text{GeV}]$. The error bands are obtained by varying the parameters within their 1σ uncertainties.

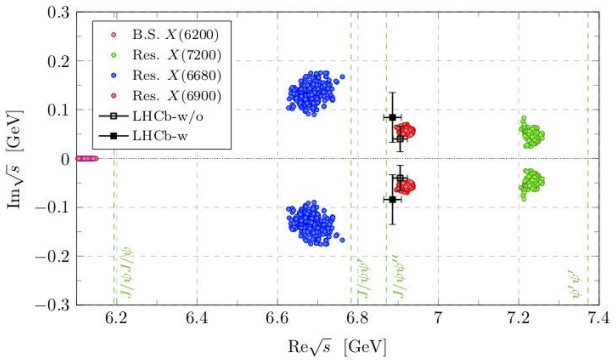

FIGURE 3. Poles locations extracted from the four-coupled-channel fits. The green dashed lines represent various thresholds. In the figure the abbreviations $\psi' = \psi(2S)$ and $\psi'' = \psi(3770)$ are used for brevity. The dots with error bars represent the LHCb results with (LHCb-w) and without (LHCb-w/o) interferences, which are shown for easy comparison.

Results of dynamically generated poles and residues, based on the four-coupled-channel fits, are detailed in Table I. It is worth mentioning that the states obtained in Fit-I and Fit-II are of quantum numbers $J^{PC} = 0^{++}$ and 2^{++}, respectively. In Fig. 3, the pole locations in the complex $\sqrt{s}$ plane are plotted, where the LHCb determinations are displayed for easy comparison. From Fig. 3, it is shown that our extraction of the $X(6900)$ state is consistent with the LHCb results within 1-σ uncertainties.

It should be noted by ending this section that a combined fit (Fit-E in Ref. [19]) with both 0^{++} and 2^{++} partial waves is performed to assess the stability of the above four-coupled-channel results. The $J/\psi\psi(3770)$ channel is switched off on purpose. It is found that the existences of the $X(6900)$ state is robust. Nevertheless, the $X(7200)$ resonance disappears but leaves remnant signal of sharp changings around 7.3 GeV in the line shape. This observation implies that the $J/\psi\psi(3770)$ channel is of crucial importance in dynamically generating the $X(7200)$ state.

5. Summary

In summary, we explore all possible states in the LHCb di-J/ψ spectrum by performing a partial-wave analysis with coupled-channel dynamics. Four states are found: two states ($X(6200)$ and $X(7200)$) in the $J^{PC} = 0^{++}$ partial wave and the other two ($X(6680)$ and $X(6900)$) in the $J^{PC} = 2^{++}$ partial wave. Our determination of the $X(6900)$ state agrees well with the LHCb results within uncertainties. Our findings can be determined more precisely in the near future when more relevant experimental data are available.

Acknowledgments

We would like thank the organizers for their dedication to HADRON 2021. This work is supported by National Nature Science Foundations of China (NSFC) under Contract No. 11905258 and by the Fundamental Research Funds for the Central Universities under Contract No. 531118010379.

i. Proceeding for the conference "19th International Conference on Hadron Spectroscopy and Structure (HADRON 2021)" hosted by Universidad Nacional Autónoma de México, from 26th to 31st of July 2021.

1. R. Aaij *et al.* [LHCb], "Observation of structure in the J/ψ - pair mass spectrum," *Sci. Bull.* **65** (2020) 1983-1993 `https://doi.org/10.1016/j.scib.2020.08.032`.

2. R. N. Faustov, V. O. Galkin and E. M. Savchenko, "Heavy tetraquarks in the relativistic quark model," *Universe* **7** (2021) 94 `https://doi.org/10.3390/universe7040094`.

3. X. Jin, X. Liu, Y. Xue, H. Huang and J. Ping, "Strange hidden-charm tetraquarks in constituent quark models," [arXiv:2011.12230 [hep-ph]].
4. Q. F. Lü, D. Y. Chen and Y. B. Dong, "Masses of fully heavy tetraquarks $QQ\bar{Q}\bar{Q}$ in an extended relativized quark model," *Eur. Phys. J. C* **80** (2020) 871 https://doi.org/10.1140/epjc/s10052-020-08454-1.
5. G. J. Wang, L. Meng, M. Oka and S. L. Zhu, "Higher fully charmed tetraquarks: Radial excitations and P-wave states," *Phys. Rev. D* **104** 036016 (2021) https://doi.org/10.1103/PhysRevD.104.036016.
6. B. C. Yang, L. Tang and C. F. Qiao, "Scalar fully-heavy tetraquark states $QQ'\bar{Q}\bar{Q}'$ in QCD sum rules," *Eur. Phys. J. C* **81** (2021) 324 https://doi.org/10.1140/epjc/s10052-021-09096-7.
7. B. D. Wan and C. F. Qiao, "Gluonic tetracharm configuration of $X(6900)$," *Phys. Lett. B* **817** (2021) 136339 https://doi.org/10.1016/j.physletb.2021.136339.
8. Z. G. Wang, "Tetraquark candidates in the LHCb's di-J/ψ mass spectrum," *Chin. Phys. C* **44** (2020) 113106 https://doi.org/10.1088/1674-1137/abb080.
9. Q. N. Wang, Z. Y. Yang, W. Chen and H. X. Chen, "Mass spectra for the $cc\bar{b}\bar{b}$ and $bb\bar{c}\bar{c}$ tetraquark states," *Phys. Rev. D* **104** 014020 (2021) https://doi.org/10.1103/PhysRevD.104.014020.
10. F. Feng, Y. Huang, Y. Jia, W. L. Sang and J. Y. Zhang, "Exclusive radiative production of fully-charmed tetraquarks at B Factory," *Phys. Lett. B* **818** (2021) 136368 https://doi.org/10.1016/j.physletb.2021.136368.
11. Y. Q. Ma and H. F. Zhang, "Exploring the Di-J/ψ Resonances around 6.9 GeV Based on $ab\ initio$ Perturbative QCD," [arXiv:2009.08376 [hep-ph]].
12. F. Feng, Y. Huang, Y. Jia, W. L. Sang, X. Xiong and J. Y. Zhang, "Fragmentation production of fully-charmed tetraquarks at LHC," [arXiv:2009.08450 [hep-ph]].
13. Z. Zhao, K. Xu, A. Kaewsnod, X. Liu, A. Limphirat and Y. Yan, "Study of charmoniumlike and fully-charm tetraquark spectroscopy," *Phys. Rev. D* **103** (2021) 116027 https://doi.org/10.1103/PhysRevD.103.116027.
14. C. Gong, M. C. Du, Q. Zhao, X. H. Zhong and B. Zhou, "Nature of X(6900) and its production mechanism at LHCb," *Phys. Lett. B* **824** (2022), 136794 https://doi.org/10.1016/j.physletb.2021.136794.
15. Q. F. Cao, H. Chen, H. R. Qi and H. Q. Zheng, "Some remarks on $X(6900)$," *Chin. Phys. C* **45** (2021) 103102 https://doi.org/10.1088/1674-1137/ac0ee5.
16. X. K. Dong, V. Baru, F. K. Guo, C. Hanhart and A. Nefediev, "Coupled-Channel Interpretation of the LHCb Double- J/ψ Spectrum and Hints of a New State Near the $J/\psi J/\psi$ Threshold," *Phys. Rev. Lett.* **126** (2021) 132001 [erratum: *Phys. Rev. Lett.* **127** (2021) 119901] https://doi.org/10.1103/PhysRevLett.127.119901.
17. A. V. Nefediev, "X(6200) as a compact tetraquark in the QCD string model," *Eur. Phys. J. C* **81** 692 (2021) https://doi.org/10.1140/epjc/s10052-021-09511-z.
18. Z. H. Guo and J. A. Oller, "Insights into the inner structures of the fully charmed tetraquark state $X(6900)$," *Phys. Rev. D* **103** (2021) 034024 https://doi.org/10.1103/PhysRevD.103.034024.
19. Z. R. Liang, X. Y. Wu and D. L. Yao, "Hunting for states in the recent LHCb di-J/ψ invariant mass spectrum," *Phys. Rev. D* **104** (2021) 034034 https://doi.org/10.1103/PhysRevD.104.034034.
20. J. A. Oller and E. Oset, "N/D description of two meson amplitudes and chiral symmetry," *Phys. Rev. D* **60** (1999) 074023 https://doi.org/10.1103/PhysRevD.60.074023.
21. J. A. Oller and E. Oset, "Chiral symmetry amplitudes in the S wave isoscalar and isovector channels and the σ, $f_0(980)$, $a_0(980)$ scalar mesons," *Nucl. Phys. A* **620** (1997) 438-456 [erratum: *Nucl. Phys. A* **652** (1999) 407-409] https://doi.org/10.1016/S0375-9474(97)00160-7.
22. J. A. Oller and U. G. Meissner, "Chiral dynamics in the presence of bound states: Kaon nucleon interactions revisited," *Phys. Lett. B* **500** (2001) 263-272 https://doi.org/10.1016/S0370-2693(01)00078-8.
23. D. L. Yao, L. Y. Dai, H. Q. Zheng and Z. Y. Zhou, "A review on partial-wave dynamics with chiral effective field theory and dispersion relation," *Rept. Prog. Phys.* **84** 076201 (2021) https://doi.org/10.1088/1361-6633/abfa6f.
24. J. A. Oller, "Coupled-channel approach in hadron–hadron scattering," *Prog. Part. Nucl. Phys.* **110** (2020) 103728 https://doi.org/10.1016/j.ppnp.2019.103728.